2019년 8월

박사학위 논문

Effect of CD133 Expressions in Prostate Cancer Cells on Bone Meatastasis

조 선 대 학 교 대 학 원

의 학 과

선 재 명

Effect of CD133 Expressions in Prostate Cancer Cells on Bone Meatastasis

대장암세포에서 유래한 CD133 발현이 전립선암세포주의 골전이에 미치는 영향

2019년 8월 23일

조 선 대 학 교 대 학 원

의 학 과

선 재 명

Effect of CD133 Expressions in Prostate Cancer Cells on Bone Meatastasis

지도교수 문 영 래

이 논문을 의학 박사학위신청 논문으로 제출함

2019년 04월

조 선 대 학 교 대 학 원

의 학 과

선 재 명

선재명의 박사학위 논문을 인준함

위원장 조선대학교 교수 최 석 (인)

위 원 조선대학교 교수 전 제 열 (인)

위 원 조선대학교 교수 김 동 휘 (인)

위 원 조선대학교 교수 임 원 봉 (인)

위 원 조선대학교 교수 문 영 래 (인)

2019년 06월

조 선 대 학 교 대 학 원

CONTENTS

LIST OF TABLES

LIST OF FIGURES

ABSTRACT

대장암세포에서 유래한 CD133 발현이 전립선암세포주의 골전이에 미치는 영향

선 재 명

지도교수 : 문 영 래

조선대학교 대학원 의학과

목적: 뼈는 전립선 암에서 가장 흔한 전이 부위이다. 암 줄기 세포 (CSCs)는 종양 재발 및 전이에서 매우 중요한 역할을 하는 것으로 알려져 있다. 본 연구에서는 전립선 암세포 주에서 암줄기세포의 안정성을 유지하는 중요한 분자인 CD133의 이소성 과발현이 전립선암세포에서 상피 간엽 전환 (EMT)을 이행하고 마우스 전이 모델에서 골전이를 유도하는지 알아 보았다.

대상 및 방법: 본 연구에서는 전립선 암세포인 LnCaP에서 CD133의 이소성 과발현을 수행하고 CSC 관련 단백질과 발현 및 콜로니 형성 분석을 수행하였다. 또한 EMT 관련 단백질 발현, 세포 침투 및 이동 분석을 수행 하였다. 골전이에서 CD133의 역할을 연구하기 위해 CD133-LnCaP를 심장 내 접종 된 마우스에서 모니터하고 H & E 염색 및 면역 조직 화학적 연구로 골 전이를 분석 하였다. 또한, 사이토 카인 분석을 통해 골전이 동안 중추적인 역할을 하는 사이토카인을 탐색하였다.

결과: LnCaP에서 CD133의 이소성 과발현은 OCT4, NANOG 발현 및 콜로니 형성 능력

그리고 E-Cadherin의 감소 및 vimentin의 증가, 세포 이동과 같은 EMT- 특성 및 CSC 특성의 증가를 유도 하였다. 또한, CD133 과발현은 마우스 모델에서 골전이 종양의 유의한 형성을 유도하였다. 또한, MIF의 높은 발현은 CD133 과발현 된 LNCaP 접종 마우스의 종양에서 유의하게 모니터링 되었다.

결론: 종합하면, CD133은 전립선 암에서의 줄기 세포 및 EMT 특성의 조절을 통해 골전이를 촉진하였으며 MIF의 과발현을 유도하여 골 용해성 전이를 유발하였다. 이러한 결과는 전립선암의 골 전이에 관한 예후 탐색 및 진단을 위한 마커 발굴에 중요한 기초 자료로서 제공되어 질 수 있으리라 여겨진다.

색인단어: CD133, 암줄기세포, 미세환경, 전이성골종양, 상피간엽이행, 골용해

Ⅰ. INTRODUCTION

Prostate cancer (PC) is the second most commonly diagnosed form of cancer and the sixth leading cause of cancer-related deaths among men worldwide[1]. In patients with localized prostate cancer, the 5-year survival approximates 100%; however, in patients in whom distant metastases have occurred, the 5-year survival drops to 31%[2]. Like most other solid malignancies, prostate cancer can metastasize to distant organs such as liver, lungs and brain, but it has an unusually high propensity for metastasizing to the bone[3]. Thus, gaining a better understanding of the mechanisms by which prostate cancer metastasizes to the bone is critical to the development and use of therapies to improve survival of patients.

Recent identification of the critical molecular and cellular events surrounding tumor progression, invasion, and metastasis to the bone as well as other sites provide new insights in targeting advanced disease[4]. Epithelial mesenchymal transition (EMT), a cellular morphological and functional transformation that switches adherent epithelial cells to migratory mesenchymal cells, is critical for tumorigenic progression and cancer metastasis. Some research have reported that EMT could promote stem cell related properties and further generate cells with the features of tumor initiation[5]. During EMT, the tumor cell can exert influences on characteristic of stem cell, conferring invasive and migratory properties in primary tumor cells, ultimately resulting in metastasis[6].

The hypothesis that tumors depend on a small fraction of cells, called cancer stem cells (CSCs), suggests that CSCs have the ability to self-renew and to generate multiple 'mature' tumor progeny[7]. From these observations, it has been assumed that CSCs are typically dormant, and their later regrowth is responsible for metastases[8]. Primary tumors are composed of a majority of differentiated epithelial cells and of a much smaller number of cells expressing stem cell markers (i.e., prostate cancer stem cells)[9]. In addition, another studies have shown that CSCs originating from primary tumor have a high potential for invasion, self-renewal and clonogenic properties[10]. These cells can be identified by an increasing list of cancer stem cell markers including CD133, c-Met, and prostate stem cell antigen[11]. It was observed in a recent analysis, on a cohort of high-risk prostate cancer patients that the number of cancer cells positive for the a-6 and a-2 integrin subunits and the c-Met receptor in primary prostate cancer was correlated with bone metastasis progression[12].

CD133 (prominin-1), a 5-transmembrane glycoprotein, was originally recognized as a hematopoietic stem cells marker[13]. Consequently, CD133 has been considered as an important cell surface marker to represent the subpopulation of CICs in brain tumors, colon carcinoma, head and neck cancer, hepatocellular carcinoma, thyroid carcinoma and prostate carcinoma[14,15]. Previously, we have demonstrated that the up regulation of CD133 in HN-cancer cells, further, the upregulation of C133 in HNSCC cancerous tissue is correlated with the progression of EMT[16]. Nonetheless, the CD133 mediated

molecular mechanisms in regulating CICs in bone metastasis of prostate cancer is still unclear.

Therefore, the research presented herein show that CD133 plays a critical role in increasing stemness, gain of EMT, thereby promoting bone metastasis of LNCaP, PC cell line. Additionally, we tried to identify which cytokines secreted by CD133+ LNCaP play a critical role during bone metastasis of PC cells. Ultimately, we demonstrate that CD133+ PCs play a central role in bone metastasis.

II. MATERIALS AND METHODS

Cell culture

LNCaP and 293T cells were purchased in 2017, from the Korean Cell Line Bank (KCLB; no. and 21573) Korean Cell Line Research Foundation, Seoul, Korea. The cells were maintained at 37° C/5% CO_2 in RPMI 1640 (Welgene, Daegu, Korea) supplemented with 10% heat-inactivated fetal bovine serum (FBS; Gibco BRL, Grand Island, NY, USA) and 0.1% antibiotic/antimycotic solution (Welgene).

Cloning of human CD133 and establishment of stably transfected $LNCaP^{Vec}$ control cells and $LNCap^{CD133+}$ cells

HT29 colon cancer cells were used as a source of CD133. Cloning of CD133 was carried out as described previously[16]. Plasmid pcDNA3.1/NT-GFP lacking the CD133 insert was used as a transfection control. To check for the translated fusion product, 293T cells were used as a positive control.

Stable cell lines overexpressing CD133 protein were created by co-transfecting confluent LNCaP-luc cells in 100 mm plates with 20 μg of pcDNA3.1/NT-GFP::CD133 or pcDNA3.1/NT-GFP plasmid using the FuGENE HD transfection reagent as described previously[16].

Western blot analysis

When cells reached about 70% confluence, the medium was removed and they

were washed twice with PBS (pH 7.4). Next, cell lysates were prepared in 200 mL of cold lysis buffer (1% NP-40, 50 mM Tris-HCl, pH 7.5, 150 mM NaCl, 0.02% sodium azide, 150 mg/mL PMSF, 2 mg/mL aprotinin, 20 mg/mL leupeptin, and 1 mg/mL pepstatin A). Approximately 30 mg of tissue lysate was separated by 10% sodium dodecyl sulfate polyacrylamide gel electrophoresis and transferred to a polyvinylidene difluoride membrane (Amersham, Piscataway, NJ, USA). Each membrane was blocked for 0.5 h with a blocking solution containing 5% skim milk in Tris-buffered saline-Tween (TBST; 2.42 g/L Tris-HCl, 8 g/L NaCl, 0.1% Tween 20, pH 7.6) and rinsed briefly in TBST. The membrane was incubated overnight at 4° C with the appropriate primary antibody:anti-CD133 (MyBioSource, San Diego, CA), anti-OCT-4 (1:1000; Cell Signaling Technology, Beverly, MA), anti-SOX2 (Cell Signaling Technology), anti-NANOG (Cell Signaling Technology), anti-E-Cadherin (Santa-Cruz Biotechnology), anti-Vimentin (Santa-Cruz Biotechnology), anti-TCF-4 (Cell Signaling Technology), anti-β-Catenin (Cell Signaling Technology) or anti-MIF (Cell Signaling Technology). A mouse monoclonal IgG specific for GAPDH (Santa-Cruz Biotechnology) was used as a control. Finally, the membrane were washed in TBST and the immunoreactivity of the proteins was detected using an enhanced chemiluminescence detection kit (Amersham).

Confocal microscopic analyses

Cells were counterstained with 4, 6-diamidino-2-phenylindole provided in ProLong Gold antifade mounting medium (Invitrogen, Carlsbad, CA, USA) to

visualize nuclear morphology. Digital images were captured at the Korea Basic Science Institute Gwangju Center using a TCS SP5 AOBS laser-scanning confocal microscope (Leica Microsystems, Heidelberg, Germany).

Colony-forming assays

Cells were seeded at a density of 1000 cells per well in nonadherent 24-well culture plates coated with a 10% polyHEMA (Sigma-Aldrich, St. louis, MO) solution in absolute ethanol and then dried overnight. After seeding, cells were incubated in a serum-free DMEM medium supplemented with 200 ng/mL EGF (Sigma-Aldrich), 20 ng/mL basic FGF (Sigma-Aldrich), and B-27 supplement (Invitrogen). After 5 days of incubation, the number of spheroids in each well was counted under a light microscope (Zeiss, Zena, Germany).

Cell migration assay

The cells were seeded into 6-well plates at a density of 1×10^5 cells/well and cultured to 90% confluence in DMEM supplemented with 10% FBS for 24 hours. The media were removed from the wells, and a straight transverse line through the adherent cells was drawn using a ruler and a sterile plastic 200 μL micropipette tip, resulting in a uniform gap. Serum-free DMEM was added, and the distances between the gaps were measured after 0 and 24 hours following capture of six random microscopic fields. Distance at 0 hours was defined as 100%.

Cell invasion assay

Cell invasion was measured using a Chemotaxis chamber (Neuro Probe, Gaithersburg, MD, USA). The cells (5×10^4 in 0.35 ml of serum-free DMEM) were loaded into the top chamber of a 10-well invasion chamber assay plate. Subsequently, DMEM supplemented with 10% FBS was placed in the lower chamber, and a matrigel-coated membrane was inserted between the two chambers. After incubation for 24 hours at 37° C, the membranes were fixed and stained with a hemacolor rapid staining kit (Merck, Darmstadt, Germany). Cells from five random microscopic fields (each 0.5 mm^2) were counted using a hematocytometer under a light microscope (Zeiss).

Immunofluorescence

To confirmed morphological changes, cells were washed three times in PBS, fixed in 4 % paraformaldehyde for 10 min at room temperature, and permeabilized with PBS containing 0.25 % of Triton X-100 (PBST) for 10-15 min at room temperature. After three washes with PBS, cells were blocked with 1 % bovine serum albumin (BSA) for 30 min. Samples were incubated overnight at 4 ◦C with respect antibody (anti-F actin; 1:500, Santa Cruz Biotechnology, anti-MIF; 1:500, Cell Signaling Technology) antibodies for 2 h at room temperature. After three washes with PBS, immune-labeled cells were counterstained with 50 μL of DAPI at 37 ◦C for 10 min. Cells were analyzed with a laser scanning confocal microscope (Leica).

Immunoprecipitation

Immunoprecipitation analysis was carried out as described previously[17]. In brief, cells were lysed in protein lysis buffer (1% [v/v] Triton X-100, 150 mM NaCl, 50 mM Tris-Cl, pH 8.0, 5 mM EDTA, and protease inhibitors) and the cell lysate was incubated with primary anti-β-Catenin antibody and protein A or G beads (GE Healthcare, Uppsala, Sweden) at 4 ° C on a rotator overnight. The beads were washed, boiled in Laemmli buffer, and processed for Western blotting.

Animals

Five-week-old male athymic nude mice (BL-6/Nu, Orient Bio Co. LTD, Seoul, Korea) were housed under controlled light conditions and fed *ad libitum*. All experimental procedures involving animals were performed in compliance with institutional and governmental requirements and were approved by the Institutional Animal Care and Use Committee (CIACUC2015-A0032), Chosun University, Gwangju, Korea.

Intra-cardiac xenograft model

Intra-cardiac injection of $LNCaP^{Vec}$ and $LNCaP^{CD133+}$ cells was used to examine the ability of PC cells to home to bone. Before injection, the cells were transfected with the pGL4.5 vector plasmid encoding luciferase (Promega, Madison, WI, USA). Stably transfected cells were further cultured in Hanks Balanced Salt Solution (Welgene) including hygromycin (2 mg/mL, Sigma-Aldrich).

Male severe combined immunodeficient mice (aged 5-6 weeks) were anesthetized with isoflurane gas. Next, $LNCaP^{Vec+}$, or $LNCaP^{CD133+}$ cells (1×10^5 per mouse) were injected into the left cardiac ventricle following a modification of the technique first described by Arguello et al[18]. The mages of tumor-bearing tissues excised from mice at necropsy were obtained 4 weeks later.

Bioluminescence imaging.

Mice were imaged for bioluminescence weekly for 4-6 weeks after intracardiac injection using the IVIS® Imaging system from PerkinElmerat the Korea Basic Science Institute (Gwangju, Korea). Images were acquired and processed using the Living Image® version 4.2 software. Anesthesia was induced with inhaled isoflurane and maintained with 2% isoflurane mixed with oxygen/nitrogen via a nose cone. D-luciferin (3 mg dissolved in water) was administered at 150 mg/kg in DPBS via intraperitoneal injection. Optical imaging was carried out ~10-15 min later.

Histologic analysis of mouse tissues

Tumor-bearing tissues were fixed in cold 4% paraformaldehyde. Bone tissue was first decalcified in sodium citrate solution before processing into histologic slides. Decalcified bones were cut at the midpoint and embedded in paraffin blocks. The fluorescence in serial paraffin sections was monitored by fluorescence microscopy (Leica Microsystems). Tissues were stained with H&E, and images were captured using a microscope slide scanner (3D-HISTECH

Ltd., Budapest, Hungary).

Cytokine profiling

The supernatant from LNCaP^{Vec} and LNCaP^{CD133+} cells and the serum from tumor bearing mouse were collected respectively and assayed using a cytokine array kit (R&D Systems), according to the instruction manual. Table 1 lists the cytokines examined using this technique. The cytokine signal was detected using an ECL detection kit (Amersham) and quantified by densitometric analysis using Image J software (Scion Corp, MD, USA).

Quantitative real-time PCR analysis

Total RNA was extracted from cells using Trizol (Invitrogen). Complementary DNA (cDNA) was synthesized from 2 μg of total RNA using the Super-Script II First-Strand Synthesis System (Invitrogen). mRNA levels were measured using quantitative real-time PCR. The glyceraldehyde-3-phosphate dehydrogenase (*Gapdh*) gene was used as an endogenous control. The sequences of the primers used to target various genes are shown in Table 2.

Immunohistochemical analysis of bone specimens

Paraffin sections were deparaffinized in three changes of xylene and rehydrated in a graded series of ethanol solutions. For antigen retrieval, slides were placed in 0.01 M citrate-buffer, pH 6.0, and heated in a steamer for 30 min. Endogenous peroxidases were quenched by incubating with 3% hydrogen

peroxide for 20 min at room temperature. Sections were incubated overnight at 4° C with a 1:50 dilution of primary antibody: anti-MIF (Santa-Cruz Biotechnology). Subsequently, sections were incubated for 30 min with a biotinylated secondary antibody (LSAB; Dako Cytomation, Glostrup, Denmark), washed in PBS, and incubated for 30 min with a streptavidin-peroxidase conjugate (LSAB, Dako Cytomation). The reaction was developed for 5 min using 3, 30-diaminobenzidine tetrahydrochloride (Sigma-Aldrich). Slides were briefly counterstained in hematoxylin, dehydrated, and cover slipped. Negative and positive controls were run simultaneously. Positive controls comprised mammary tissue. The slides were captured using a microscope slide scanner (3D-HISTECH Ltd.).

Statistical analysis

A two-tailed, paired Student t test was used for statistical analyses. A P value < 0.05 was considered statistically significant. Data are expressed as the mean ± standard deviation (SD) unless specified otherwise. Data were analyzed using the SPSS version 20.0 software program for Windows (SPSS, Chicago, IL, USA). The GraphPad Prism version 6.00 software program for Windows (GraphPad, La Jolla, CA, USA) was used to analyze data from *in vitro* and *in vivo* experiments.

III. RESULTS

Stable overexpression of CD133 in LNCaP cell lines

To determine the effect of CD133 overexpression *in vitro*, we first established stable cell lines overexpressing CD133 under the control of a constitutive promoter. Specifically, we transfected the LNCaP with either CD133 or an empty vector tagged with GFP. A representative CD133 clone was selected from $LNCaP^{CD133+}$ and then compared with a control cells transfected with the empty vector ($LNCaP^{Vec}$). $293T^{Vec}$ or $293T^{CD133+}$ which were transiently transfected were used as a positive control. Basal expression of CD133 protein by $LNCaP^{Vec}$ was very low; however, that by stable CD133-transfected cells ($LNCaP^{CD133+}$) and transiently transfected 293T cells (Fig. 1a) was apparently higher. Green fluorescence was detected in the cytosol and on the cell membrane of $LNCaP^{CD133+}$ (Fig. 1b).

To investigate the role of CD133 in cancer stemness, we examined acquisition of CSC properties, such as elevated ability to form tumorspheres and expression of stem cell-like markers such as OCT4, SOX2 and NANOG. The protein expression of OCT4 and NANOG were significantly elevated in $LNCaP^{CD133+}$ consistent with increases of stemness property (Fig. 1c). Stemness was also confirmed by colony-formation assay. Colony-forming ability was significantly elevated in $LNCaP^{CD133+}$, concordant with the elevated expression of stemness factors (Fig. 1d). These results demonstrated that increased colony forming ability and protein expression of OCT4 and Nanog were capable of inducing a stem-like

property during ectopic overexpression of CD133.

Properties related with an EMT on CD133-overexpressed LNCaP cell lines

CD133 overexpression in LNCaP led to a significant increase in cell migration and cell invasion, as determined by wound healing and cell invasion assay. After 24 hours, artificial wound gaps became significantly narrower in $LNCaP^{CD133+}$ than in $LNCaP^{Vec}$ (Fig. 2a). Also, invasion abilities of $LNCaP^{CD133+}$ were increased significantly (Fig. 2b). To monitor the morphological changes in LNCaP cells, immunofluorescence of F-actin were observed using by confocal microscope. Majority of spindle and discontiguous cells were observed in $LNCaP^{CD133+}$ in compared with $LNCaP^{Vec}$ (Fig.2c).

To search for factors associated with alterations invasiveness and migration caused by ectopic overexpression of CD133, we monitored the levels of epithelial and mesenchymal markers in prostate cancer cells. Protein expression in $LNCaP^{CD133+}$ revealed that the epithelial marker E-cadherin was slightly lower relative to $LNCaP^{Vec}$ (Fig. 2d). By contrast, the mesenchymal markers vimentin was significantly upregulated in $LNCaP^{CD133+}$. In addition, analysis of β-catenin-associated signal transduction was carried out by immunoprecipitation in $LnCaP^{CD133+}$. Overexpression of CD133 led to significant increase the level of TCF-4 binding to β-catenin which is transcriptional factor for inducing EMT in cancer cells (Fig. 2e). As a result, these data strongly support the idea that CD133 is essential for repression of E-cadherin and expression of vimentin, leading to subsequent EMT and metastasis in

prostate cancer cells.

CD133 promotes LNCaP-induced bone metastasis *in vivo*

We injected LNCaP^{Vec} or LNCaP^{CD133+} cells into the left cardiac ventricle of male nude mice at a rate of 0.5x10^{6} cells/mouse. Since the LNCaP cell line was labeled with luciferase and GFP, metastatic tumors by bioluminescence imaging could be observed. The mice were imaged weekly beginning 4 weeks after the intracardiac injection. The whole mouse image in Fig. 3a shows the results of the injection of PBS for Mock, LNCaP^{Vec} and LNCaP^{CD133+} cells. A large hot spot and small spot of bioluminescence was observed in whole body following LNCaP^{CD133+} cell injection. Table 3 shows that only 20% of animals inoculated with LNCaP^{Vec} cells developed skeletal tumors (n = 10) compared with 80% inoculated with LNCaP^{CD133+}.

Next, we performed H&E staining to examine the histologic features of skeletal tumors formed by LNCaP^{Vec}/LNCaP^{CD133+} cells inoculated into mouse cardiac. As shown in Figure 3b, gross examination of excised spine in both of LNCaP^{Vec} and LNCaP^{CD133+} cells inoculated into mouse cardiac revealed that in general the tumor mass occupied the primary spongiosum (trabecular epiphysis) and displaced the bone marrow cells. In particular, there was an apparent margin between spinal cord and metastatic tumors in LNCaP^{Vec}-inoculated mouse; however, metastatic tumors invasion into spinal cord and discursive osteolytic features of vertebrae were observed in LNCaP^{CD133+}-inoculated mouse.

Next, we tried to identify the released molecules that play a critical role of LNCaP^{CD133+} in bone metastatic development by screening cytokines using a proteome array cytokine kit (Fig. 3c). Overexpression of CD133 by LNCaP cells led to a marked increase in release of IL-8 and macrophage migration inhibitory factor (MIF) from mouse serum. Especially, MIF were either increased in cell supernatant of LNCaP^{CD133+}. These data suggest that ectopic overexpression of CD133 leads to a significant increase the risk of bone metastatic cancer, and that increased MIF may contribute the PC metastasis to the bone.

Expression of MIF in primary PCs and metastatic lesion

To investigate the role of MIF during bone metastasis of LNCaP cells, mRNA and protein expression of MIF were analyzed. Indeed, levels of MIF protein (Fig. 4a) and mRNA (Fig. 4b) were higher in LNCaP^{CD133+} cells than in LNCaP^{Vec} cells. To monitor the cellular distribution of MIF in LNCaP cells, immunofluorescence of MIF were observed using by confocal microscope. The MIF expression were in the membrane and cytosol were observed in LNCaP^{CD133+} in compared with LNCaP^{Vec} (Fig.4c).

In the immunohistochemical study, strong expression of MIF were observed around the tumor mass and trabecular epiphysis region of bone inoculated with LNCaP^{CD133+} cells. These observations suggest that ectopic overexpression of CD133 leads to increase the MIF release from CD133+ cells and activation of bone adjacent to the tumor, particularly in bone injected with LNCaP cells, and that CD133 expression is associated with metastasis of PC to bone.

IV. DISCUSSION

Bone is a common site of distant metastasis in prostate cancer. Association of bone and metastatic cancer cells are important in this site-specific manifestation of prostate cancer progression[19]. Despite the advances in understanding the mechanisms of the basic molecular biology of bone metastasis there are no curative treatments for the disease at this stage and bone metastasis remains a devastating complication of advanced prostate cancer. During the last decades, the existence and the identity of CSCs suggested that played a pivotal role in its metastasis[20]. In this study, we first sought to identify CSC-like cells by ectopic overexpression of CD133 in prostate cancer cell lines, LNCaP. It led the genetic changes in prostate cancer cells altered the expression of several factors related to stemness, including OCT4, and NANOG, resulting in increased colony-forming abilities. Furthermore, genetic modulation of CD133 altered the expression of EMT-related factors, increased vimentin and decreased E-cadherin, resulted in generation of complex with TCF-4 and β-catenin. Although the role of EMT in prostate cancer remains unclear, several factors involved in EMT or related programs have been revealed as key molecules in cancer cell invasion and metastasis. The strong correlation between CD133 and EMT factors may therefore explain the elevated invasiveness and migration of $LNCaP^{CD133+}$. Recent studies have shown that EMT can induce differentiated cancer cells into a CSC-like state. The EMT has been described over the past decade as a critical normal process during development and wound

healing, but recently properties of EMT have been implicated in human pathology, including cancer metastasis[21]. However, no research has yet revealed the mechanisms behind them, or identified the source of the cells with both EMT for bone metastasis and stem cell properties. In this study, we demonstrate for the first time that prostate cancer cells can acquire mesenchymal characteristics and stem cell properties by ectopic overexpression of CD133. These observations suggested that CSCs may underlie local and distant metastases to the bone by acquiring mesenchymal features which would greatly facilitate systemic dissemination from the primary mass. Also, during the process of tumor metastasis, redundant regulation of β-catenin/TCF-4 signaling through several EMT-inducing signals propose that its expression is key in the initiation and maintenance of the EMT process. Recent evidence has shown that the microenvironment at the invasive front of cancer cells and, more specifically, secretion of factors like hepatocyte growth factor by stromal myofibroblasts in the vicinity of dedifferentiated cancer cells play an important role in the nuclear translocation of β-catenin and activation of β-catenin/TCF signaling[17]

Then, which factors play a critical role in CD133+ PC cell-induced bone metastasis? To answer the question, $LNCaP^{Vec}$ and $LNCaP^{CD133+}$ cells were inoculated into intracardiac of athmic nu/mouse and released cytokines with paracrine and endocrine action in mouse serum were investigated by array kit. In histologic finding, CD133+ cells generated bigger and more aggressive tumor mass than wild type and $LNCaP^{CD133+}$ cells showed higher expression of MIF than $LNCaP^{Vec}$,

suggesting that MIF elicits essential biological functions and may play a critical role of bone metastasis of PC. MIF is a pleiotropic inflammatory cytokine with chemokine-like functions that can bind and signal via several receptors including CD74, CXCR2, and CXCR4[22]. Especially, MIF is known to induce the osteoclast differentiation and contribute the progression of various bone and periodontal disease[23]. The previous studies also showed that ligation of both MIF and SDF-1 chemokines to CXCR4 receptor, triggers chemotaxis of OCPs and enhances osteoclastogenesis[24]. The interaction of MIF with chemokine receptors can at least explain its ability to induce macrophage migration and osteoclastogenesis. Our current findings lend support to the conclusion that, while a physiological target has yet to be identified, the tautomerase activity is important for functions of MIF that contribute to its role in tumor growth and metastasis. The tropism of LNCaP^{CD133+} cells to bone suggests that CSCs may preferentially interact with specific cells in the bone microenvironment, the most likely candidates of which are osteoclast, resulted in increased bone lysis in the sites of bone metastases with histomorphometric evidences.

For the clinical applications, CD133 may be a candidate marker for the diagnosis of possibility of bone metastasis in prostate cancer patients. The inability to predict which patients will develop metastatic disease remains a major challenge for prostate cancer management and has resulted in excessive therapy for some patients and delayed or insufficient therapy for others[25]. Although the presence of circulating prostate cancer cells in the blood is an

indication that tumor cells have disseminated from the primary site, the nature of the association between circulating tumor cells and bone metastasis remains controversial. It is possible that only a subset of circulating tumor cells possesses the necessary properties to target bone.

V. CONCLUSION

In light of significant advances in metastasis and stem cell research, we propose a CSC-based model for bone metastasis of prostate cancer. Our findings indicate that CD133 plays a functional role in regulating cancer stem cell and EMT properties in prostate cancer and sustained acquisition of osteolytic features by MIF secretion. These data substantiate the role of EMT and support the role of CSCs in cancer metastasis to the bone. Therefore, our results should facilitate development of a novel classification system and therapeutic strategies for bone metastasis.

REFERENCES

1. Hassanipour-Azgomi S, Mohammadian-Hafshejani A, Ghoncheh M, Towhidi F, Jamehshorani S, Salehiniya H. Incidence and mortality of prostate cancer and their relationship with the Human Development Index worldwide. Prostate Int. 2016;4:118-24.

2. Jemal A, Siegel R, Xu J, Ward E. Cancer statistics, 2010. CA Cancer J Clin. 2010;60:277-300.

3. Jin JK, Dayyani F, Gallick GE. Steps in prostate cancer progression that lead to bone metastasis. Int J Cancer. 2011;128:2545-61.

4. Nakazawa M, Kyprianou N. Epithelial-mesenchymal-transition regulators in prostate cancer: Androgens and beyond. J Steroid Biochem Mol Biol. 2016;

5. Chen YS, Wu MJ, Huang CY, et al. CD133/Src axis mediates tumor initiating property and epithelial-mesenchymal transition of head and neck cancer. PLoS One. 2011;6:e28053.

6. Yilmaz M, Christofori G. EMT, the cytoskeleton, and cancer cell invasion. Cancer Metastasis Rev. 2009;28:15-33.

7. Al-Hajj M, Wicha MS, Benito-Hernandez A, Morrison SJ, Clarke MF. Prospective identification of tumorigenic breast cancer cells. Proc Natl Acad Sci U S A. 2003;100:3983-8.

8. Shiozawa Y, Berry JE, Eber MR, et al. The marrow niche controls the cancer stem cell phenotype of disseminated prostate cancer. Oncotarget. 2016;

9. Klonisch T, Wiechec E, Hombach-Klonisch S, et al. Cancer stem cell markers

in common cancers - therapeutic implications. Trends Mol Med. 2008;14:450-60.

10. Yu C, Yao Z, Jiang Y, Keller ET. Prostate cancer stem cell biology. Minerva Urol Nefrol. 2012;64:19-33.

11. Kryczek I, Liu S, Roh M, et al. Expression of aldehyde dehydrogenase and CD133 defines ovarian cancer stem cells. Int J Cancer. 2012;130:29-39.

12. Colombel M, Eaton CL, Hamdy F, et al. Increased expression of putative cancer stem cell markers in primary prostate cancer is associated with progression of bone metastases. Prostate. 2012;72:713-20.

13. Shmelkov SV, St Clair R, Lyden D, Rafii S. AC133/CD133/Prominin-1. Int J Biochem Cell Biol. 2005;37:715-9.

14. Major AG, Pitty LP, Farah CS. Cancer stem cell markers in head and neck squamous cell carcinoma. Stem Cells Int. 2013;2013:319489.

15. Collins AT, Berry PA, Hyde C, Stower MJ, Maitland NJ. Prospective identification of tumorigenic prostate cancer stem cells. Cancer Res. 2005;65:10946-51.

16. Moon Y, Kim D, Sohn H, Lim W. Effect of CD133 overexpression on the epithelial-to-mesenchymal transition in oral cancer cell lines. Clin Exp Metastasis. 2016;33:487-96.

17. Sanchez-Tillo E, de Barrios O, Siles L, Cuatrecasas M, Castells A, Postigo A. beta-catenin/TCF4 complex induces the epithelial-to-mesenchymal transition (EMT)-activator ZEB1 to regulate tumor invasiveness. Proc Natl Acad Sci U S A. 2011;108:19204-9.

18. Arguello F, Baggs RB, Frantz CN. A murine model of experimental metastasis

to bone and bone marrow. Cancer Res. 1988;48:6876-81.

19. Valta MP, Tuomela J, Bjartell A, Valve E, Vaananen HK, Harkonen P. FGF-8 is involved in bone metastasis of prostate cancer. Int J Cancer. 2008;123:22-31.

20. Lee KH, Ahn EJ, Oh SJ, et al. KITENIN promotes glioma invasiveness and progression, associated with the induction of EMT and stemness markers. Oncotarget. 2015;6:3240-53.

21. Xu MH, Gao X, Luo D, Zhou XD, Xiong W, Liu GX. EMT and acquisition of stem cell-like properties are involved in spontaneous formation of tumorigenic hybrids between lung cancer and bone marrow-derived mesenchymal stem cells. PLoS One. 2014;9:e87893.

22. Pasqualon T, Lue H, Groening S, et al. Cell surface syndecan-1 contributes to binding and function of macrophage migration inhibitory factor (MIF) on epithelial tumor cells. Biochim Biophys Acta. 2016;1863:717-26.

23. Madeira MF, Queiroz-Junior CM, Costa GM, et al. MIF induces osteoclast differentiation and contributes to progression of periodontal disease in mice. Microbes Infect. 2012;14:198-206.

24. Movila A, Ishii T, Albassam A, et al. Macrophage Migration Inhibitory Factor (MIF) Supports Homing of Osteoclast Precursors to Peripheral Osteolytic Lesions. J Bone Miner Res. 2016;31:1688-700.

25. Chu K, Cheng CJ, Ye X, et al. Cadherin-11 promotes the metastasis of prostate cancer cells to bone. Molecular cancer research : MCR. 2008;6:1259-67.

Table 1. List of human inflammatory cytokines examined using the antibody array (R&D Systems)

Coordinate	Analyte/Control	Entrez Gene ID	Alternate Nomenclature
A1, A2	Reference Spots	N/A	RS
A3, A4	Adiponectin	9370	Acrp30
A5, A6	Apolipoprotein A-I	335	ApoA1
A7, A8	Angiogenin	283	_____
A9, A10	Angiopoietin-1	284	Ang-1, ANGPT1
A11, A12	Angiopoietin-2	285	Ang-2, ANGPT2
A13, A14	BAFF	10673	BLyS, TNFSF13B
A15, A16	BDNF	627	Brain-derived Neurotrophic Factor
A17, A18	Complement Component C5/C5a	727	C5/C5a
A19, A20	CD14	929	_____
A21, A22	CD30	943	TNFRSF8
A23, A24	Reference Spots	N/A	RS
B3, B4	CD40 ligand	959	CD40L, TNFSF5, CD154, TRAP
B5, B6	Chitinase 3-like 1	1116	CHI3L1, YKL-40
B7, B8	Complement Factor D	1675	Adipsin, CFD
B9, B10	C-Reactive Protein	1401	CRP
B11, B12	Cripto-1	6997	Teratocarcinoma-derived Growth Factor
B13, B14	Cystatin C	1471	CST3, ARMD11
B15, B16	Dkk-1	22943	Dickkopf-1
B17, B18	DPPIV	1803	CD26, DPP4, Dipeptidyl-peptidase IV
B19, B20	EGF	1950	Epidermal Growth Factor
B21, B22	Emmprin	682	CD147, Basigin
C3, C4	ENA-78	6374	CXCL5
C5, C6	Endoglin	2022	CD105, ENG
C7, C8	Fas Ligand	356	TNFSF6, CD178, CD95L
C9, C10	FGF basic	2247	FGF-2

C11, C12	FGF-7	2252	KGF
C13, C14	FGF-19	9965	_____
C15, C16	Flt-3 Ligand	2323	FLT3LG
C17, C18	G-CSF	1440	CSF3
C19, C20	GDF-15	9518	MIC-1
C21, C22	GM-CSF	1437	CSF2
D1, D2	GRO α	2919	CXCL1, MSGA-α
D3, D4	Growth Hormone	2688	GH, Somatotropin
D5, D6	HGF	3082	Scatter Factor, SF
D7, D8	ICAM-1	3383	CD54
D9, D10	IFN-γ	3458	IFNG
D11, D12	IGFBP-2	3485	_____

Table 2. Gene primer sequences

Gene name	Upstream primer (5’-3’)	Downstream primer (3’-5’)
MIF	GGA CAG CCA GGA CTC CAT TG	TGT GGG GAC AAC TGG AGT GA
GAPDH	TGG AAT CCA CTG GCG TCT TC	GGT TCA CGC CCA TCA CAA AC

Table 3. Characteristics of the tumor formations.

Cell Line	Injection	Cell No.	Tumor formation
$LNCaP^{Vec}$	Intracardiac	1×10^5	2/10 (20%)
$LNCaP^{CD133+}$	Intracardiac	1×10^5	8/10 (80%)

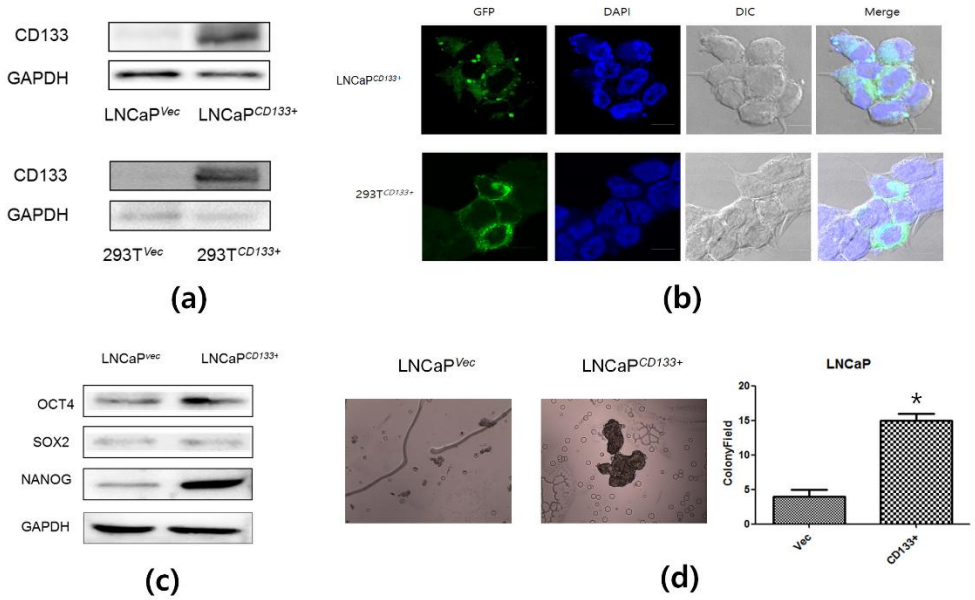

Figure 1. Overexpression of CD133 in prostate cancer cell lines. (a) Western blot analysis of CD133 expression by $LNCaP^{Vec}$ (controls) and $LNCaP^{CD133+}$ (CD133-overexpressing) cells. 293T cells transiently transfected with pcDNA3.1/NT-GFP or pcDNA3.1/NTGFPCD133. $293T^{Vec}$/$293T^{CD133+}$ cells were used as a positive control. (b) Confocal microscopy analysis of GFP-CD133 expression by stably or transiently transfected LNCaP/293T-GFP-CD133 cells. Nuclei in both sets of images are stained with DAPI (blue). Images were taken at 630× magnification. Bar, 10 μm. (c) Western blot analysis of expression of stemness-related proteins. GAPDH was used as a loading control. Similar results were obtained in three separate experiments. (d) Stable overexpression of CD133 led to a significant increase in colony-forming ability. Images were taken at 100× magnification. Bar, 100 μm. Bar graphs showing the mean ± the standard deviation (SD). *, $P < 0.05$.

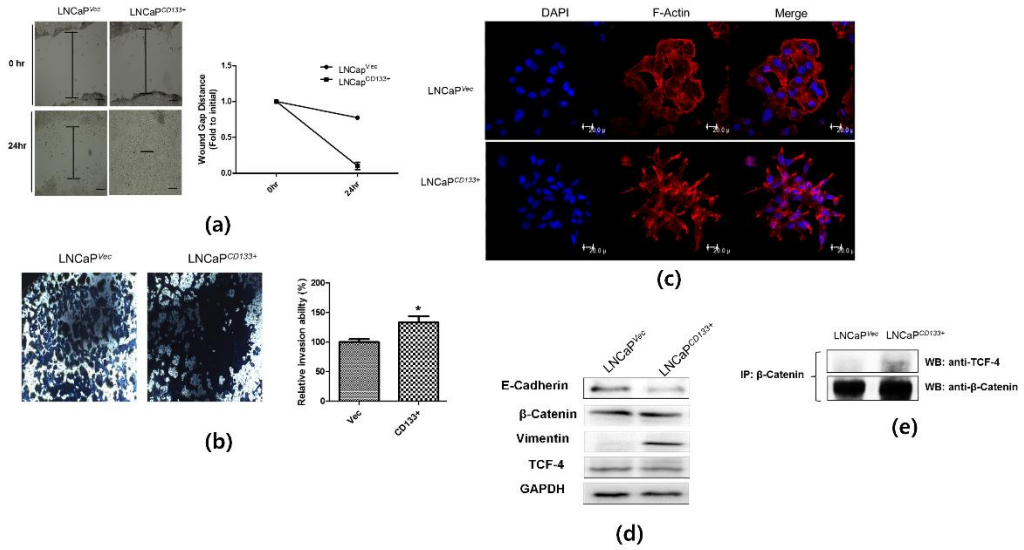

Figure 2. CD133 overexpression promotes EMT in LNCaP cells. (a) CD133 overexpression led to a significant increase in the migratory capacity of LNCaP cells, as shown by the reduced wound gap distance at 24 h. Images were taken at 100× magnification. Bar, 100 μm. The data in the associated graphs are expressed as the mean ± the standard deviation (SD). (b) CD133 overexpression significantly increases the invasiveness of LNCaP cells. Images were taken at 100× magnification. Bar, 100 μm. Data in the associated bar graphs are expressed as the mean ± the SD. (c) Confocal microscopy of F-actin expression in LNCaP cells. Nuclei in respect sets of images were stained with DAPI (blue). Images were taken at 630× magnification. Bar,20 um. (d) Expression of EMT-related proteins was characterized by western blotting. GAPDH was used as a loading control. Results are representative of three separate experiments, all with similar results. (e) Immunoprecipitation of β-catenin

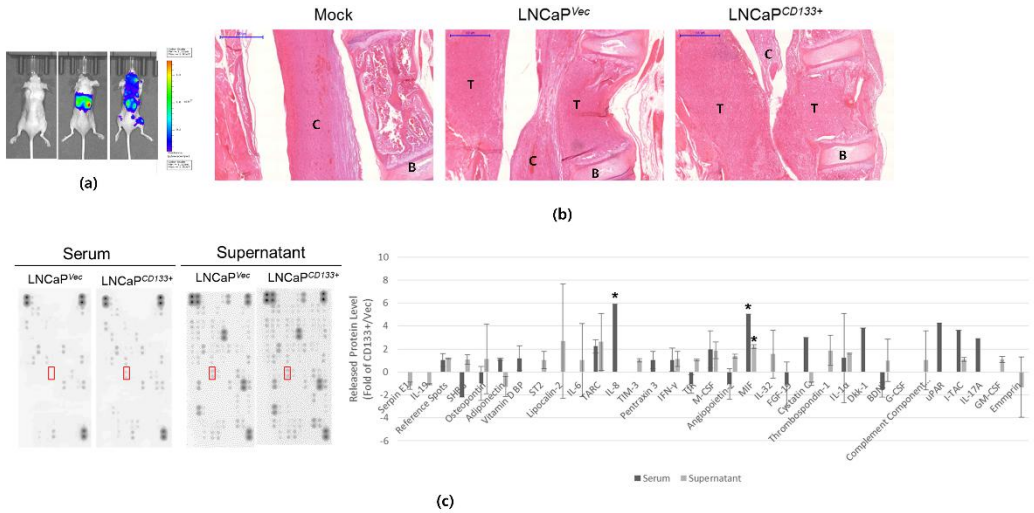

Figure 3. Comparison of tumor-bearing mouse (a) Tumor growth and multiple metastases were monitored over time by *in vivo* bioluminescence imaging. Data for a representative mouse are shown. A large hot-spot of bioluminescence observed in vivo following inoculation with the LNCaP^{Vec} cell line. Induction of multiple localized and distant metastases *in vivo* after injection of LNCaP^{CD133+} cells into the heart of nude mice. Colored bar indicates the bioluminescence signal intensity range (photon/sec/cm2/steradian). (b) Hematoxylin and eosin staining of mouse tissue sections at the end of the study period. Representative histological sections of spine tissues were shown in metastasis. (200× magnification; bar, 100 μm) magnification. B, Bone; T, Tumor mass; C; Spinal cord. (c) Cytokine profiling of LNCaP^{Vec}/LNCaP^{CD133+}. Culture supernatant from each cell line and serum from each mouse were harvested after 24 h and assayed using a cytokine profile array kit. The bar represents the mean ratio ± SD from two experiments. Significant differences were seen at *P < 0.05.

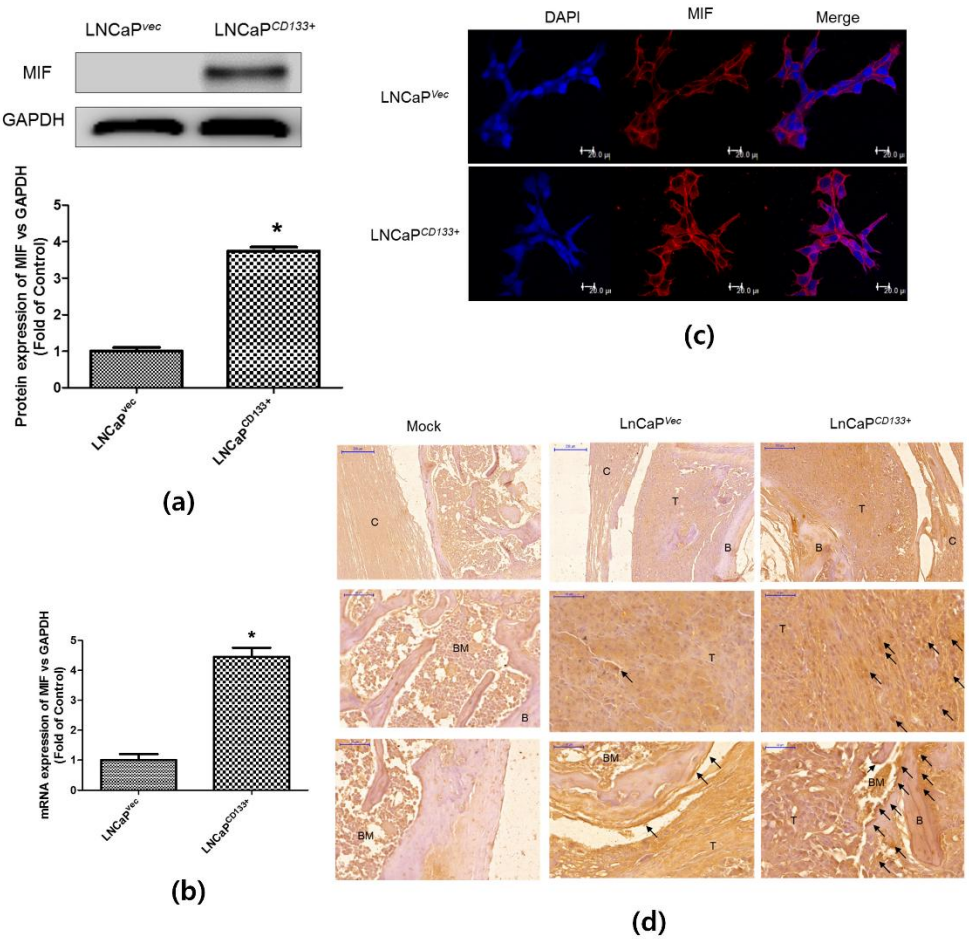

Figure 4. Expression of MIF in LNCaP^{Vec} and LNCaP^{CD133+} for in vitro and in vivo study. (a) Expression of OPN protein in LNCaP^{Vec} and LNCaP^{CD133+} cells was measured by western blotting. GAPDH was used as a loading control. (b) MIF mRNA expression in LNCaP^{Vec} and LNCaP^{CD133+} cells was characterized by real-time PCR. *, $P < 0.05$. (c) Confocal microscopy of MIF expression in LNCaP cells. Nuclei in respect sets of images were stained with DAPI (blue). Images were

taken at 630× magnification. Bar, 20 um. (d) Immunohistochemical study of MIF in mouse tissue sections at the end of the study period. Representative histological sections of spine tissues were shown in metastasis. (200× magnification; bar, 100 μm) magnification. B, Bone; T, Tumor mass; C; Spinal cord.